Supplementary Information

Intermetallics triggering pyroptosis and disulfidptosis in cancer cells promote anti-tumor immunity

Yanlin Zhu,[1] Xinxin Wang,[2] Lili Feng,[1,] Ruoxi Zhao,[1] Can Yu,[2] Yuanli Liu,[3] Ying Xie,[4] Bin Liu,[1] Yang Zhou,[2,*] and Piaoping Yang[1,*]*

[1]Key Laboratory of Superlight Materials and Surface Technology, Ministry of Education, College of Materials Science and Chemical Engineering, Harbin Engineering University, Harbin 150001, P. R. China.
[2]Department of Radiology, Harbin Medical University Cancer Hospital, Harbin 150000, P. R. China.
[3]Department of Biochemistry and Molecular Biology, Harbin Medical University, Harbin 150086, P. R. China.
[4]Key Laboratory of Functional Inorganic Material Chemistry, Ministry of Education, School of Chemistry and Materials Science, Heilongjiang University, Harbin, 150080, P. R. China

Correspondence and requests for materials should be addressed to L.F. (email: fenglili@hrbeu.edu.cn), Y. Zhou (email: Zhouyang094@126.com), or P.Y. (email: yangpiaoping@hrbeu.edu.cn).

Supplementary Figures

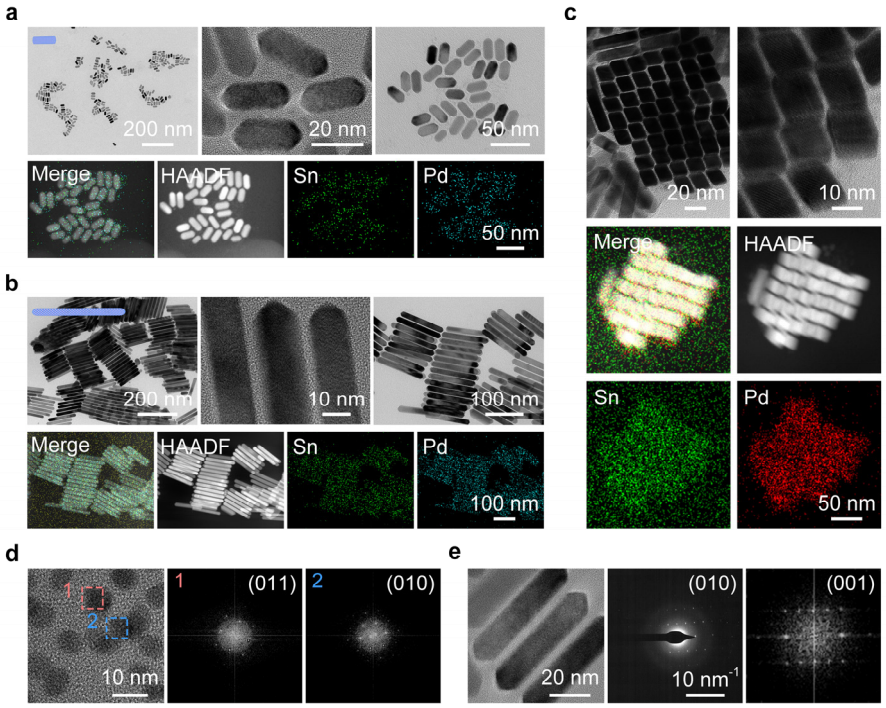

Supplementary Fig. 1. Characterization of Pd_2Sn NRs. TEM images and the corresponding elemental mapping of **a** Pd_2Sn SNRs, **b** Pd_2Sn LNRs, and **c** end face of Pd_2Sn NRs. HRTEM images and the corresponding Fast Fourier Transform patterns of **d** Pd_2Sn NDs and **e** Pd_2Sn NRs. (one representative data was shown from six independently repeated experiments).

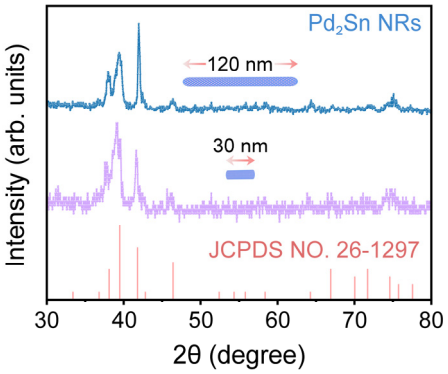

Supplementary Fig. 2. Powder XRD patterns of Pd_2Sn LNRs and Pd_2Sn SNRs (n = 3 independent experiments). Source data are provided as a Source Data file (arb. units, arbitrary units).

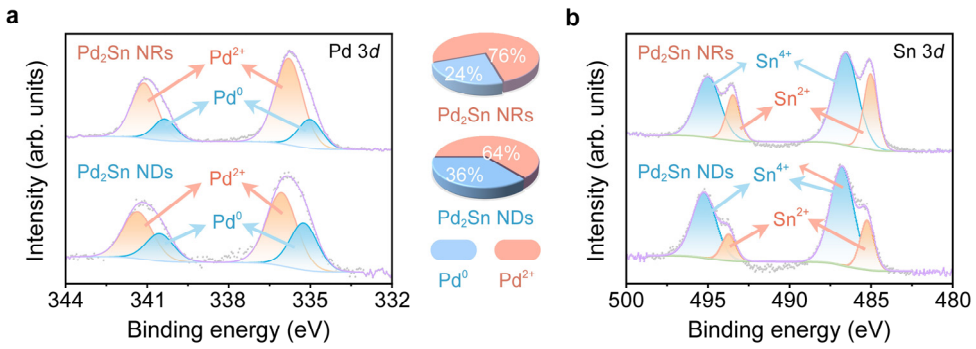

Supplementary Fig. 3. High-resolution XPS spectra. High-resolution XPS spectra of **a** Pd 3*d* and **b** Sn 3*d* for Pd_2Sn NRs and Pd_2Sn NDs after prolonged oxidation (n = 3 independent experiments). Source data are provided as a Source Data file (arb. units, arbitrary units).

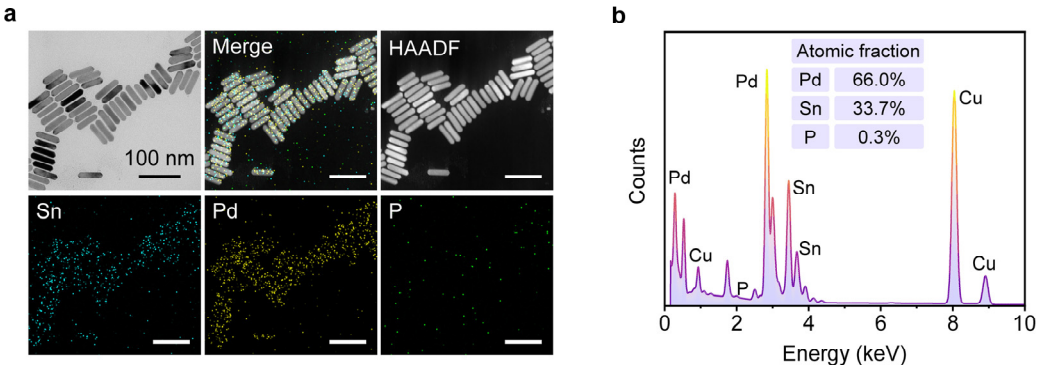

Supplementary Fig. 4. Characterization of Pd_2Sn NRs. a TEM image and corresponding elemental mapping of Pd_2Sn NRs. (one representative data was shown from six independently repeated experiments). **b** EDS spectrum of Pd_2Sn NRs. Source data are provided as a Source Data file.

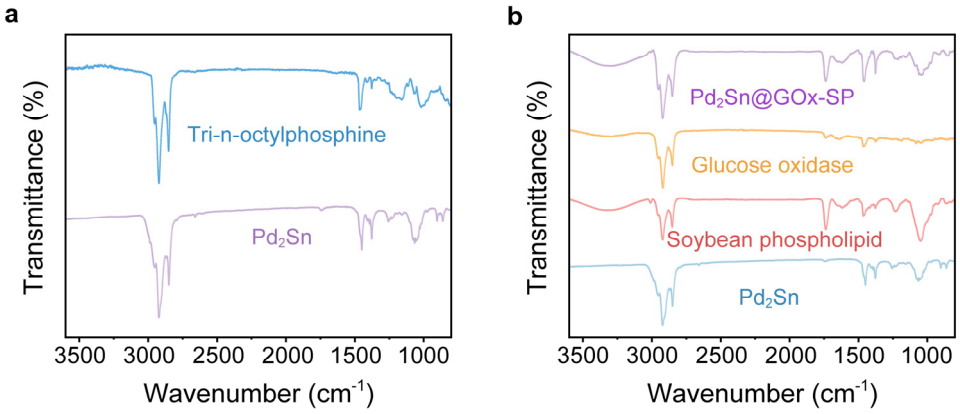

Supplementary Fig. 5. FT-IR spectra. The FT-IR spectra of **a** Pd_2Sn, tri-n-octylphosphine, and **b** soybean phospholipid, glucose oxidase, Pd_2Sn@GOx-SP, respectively (n = 3 independent experiments). The peaks from 1800 to 1500 cm^{-1} in the Pd_2Sn@GOx-SP sample indicated the successful modification of soybean phospholipid. Source data are provided as a Source Data file.

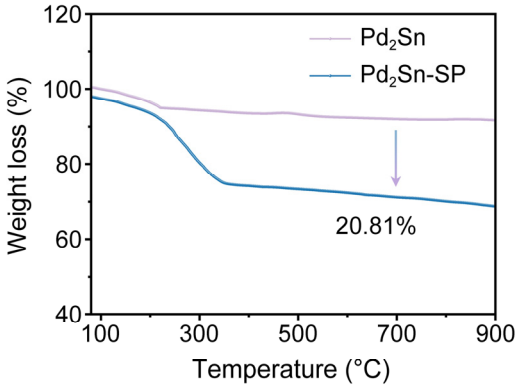

Supplementary Fig. 6. TGA curves obtained from Pd_2Sn and Pd_2Sn-SP (n = 3 independent experiments). Source data are provided as a Source Data file.

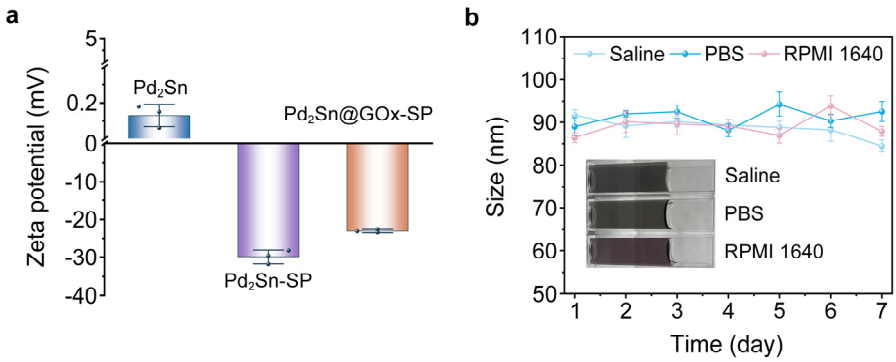

Supplementary Fig. 7. Zeta potentials and particle size analysis. a The zeta potentials of Pd_2Sn, Pd_2Sn-SP, and Pd_2Sn@GOx-SP nanocomposites. **b** Hydrodynamic dimension changes of Pd_2Sn@GOx-SP nanocomposites dispersed in different physiological solutions for one week. Data are expressed as mean ± S.D. (n = 3 independent experiments). Source data are provided as a Source Data file.

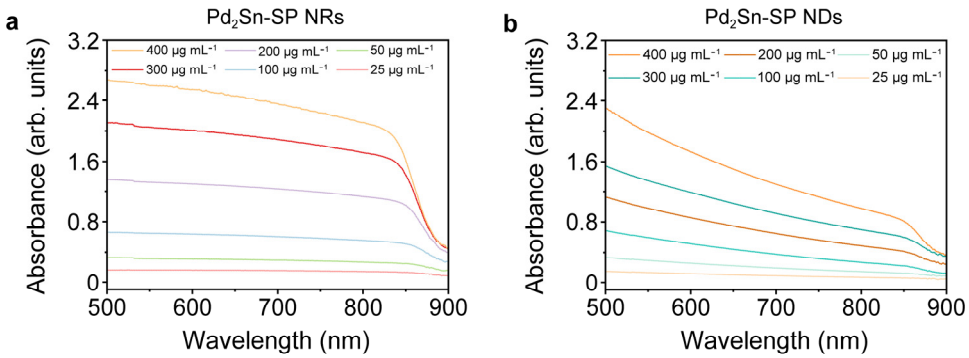

Supplementary Fig. 8. UV-vis-NIR absorption spectra. **a** Pd_2Sn-SP NRs, **b** Pd_2Sn-SP NDs (n = 3 independent experiments). Source data are provided as a Source Data file (arb. units, arbitrary units).

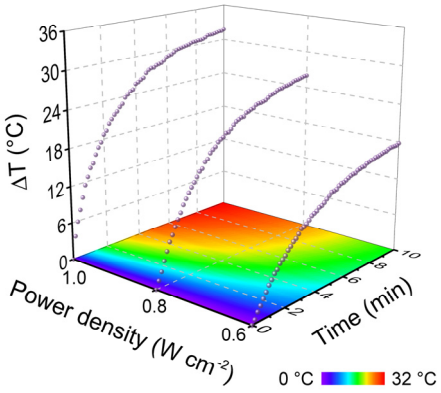

Supplementary Fig. 9. Photothermal heating curves of Pd_2Sn-SP NRs irradiated upon 808 nm laser in various power densities (n = 3 independent experiments). Source data are provided as a Source Data file.

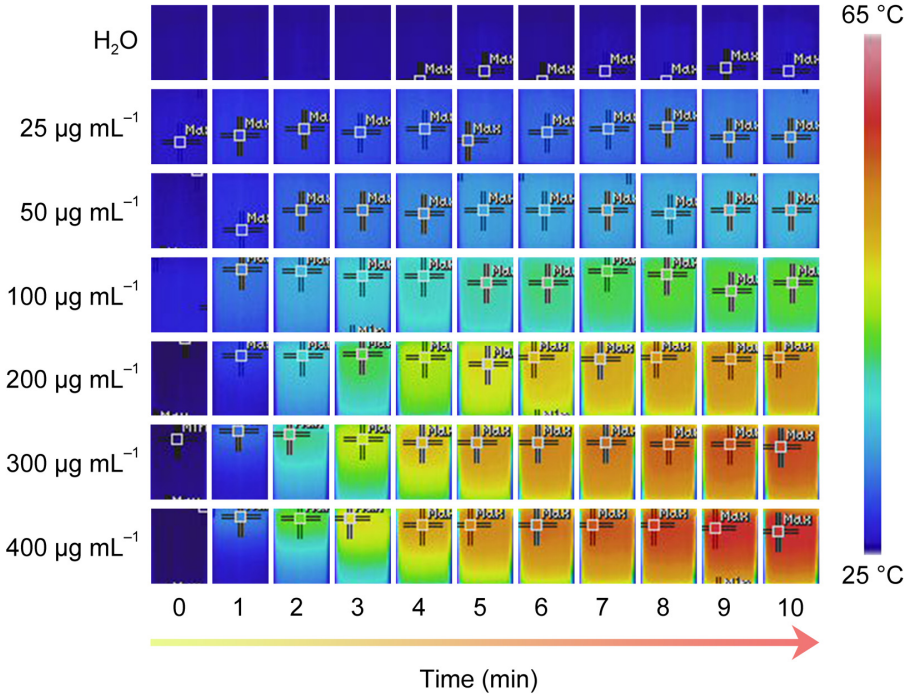

Supplementary Fig. 10. Infrared thermal images of pure water and Pd_2Sn-SP NRs with various concentrations irradiated upon 808 nm laser (n = 3 independent experiments).

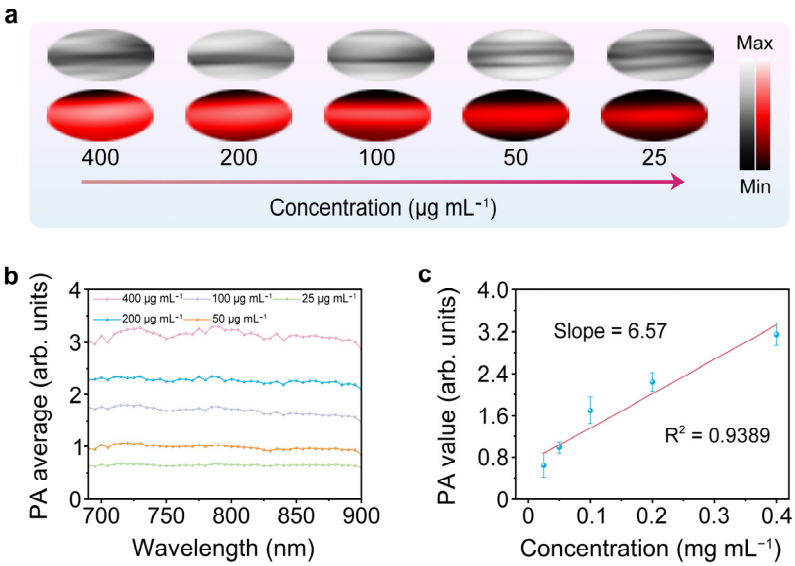

Supplementary Fig. 11. In vitro PA imaging. a In vitro PA images Pd_2Sn-SP with different concentrations. **b** The average PA signal intensity and **c** the corresponding linear fitting of Pd_2Sn-SP with different concentrations at 808 nm. Data are expressed as mean ± S.D. (n = 3 independent experiments). Source data are provided as a Source Data file (arb. units, arbitrary units).

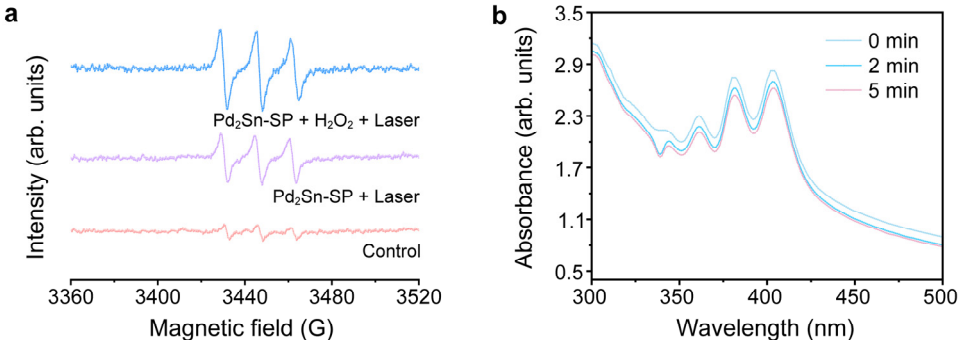

Supplementary Fig. 12. In vitro $^1O_2$ generation by Pd_2Sn-SP. a ESR spectra of $^1O_2$ trapped by TEMP under different conditions. **b** UV-vis spectra of DPA degradation in the presence of Pd_2Sn-SP irradiated with 808 nm laser (n = 3 independent experiments). Source data are provided as a Source Data file (arb. units, arbitrary units).

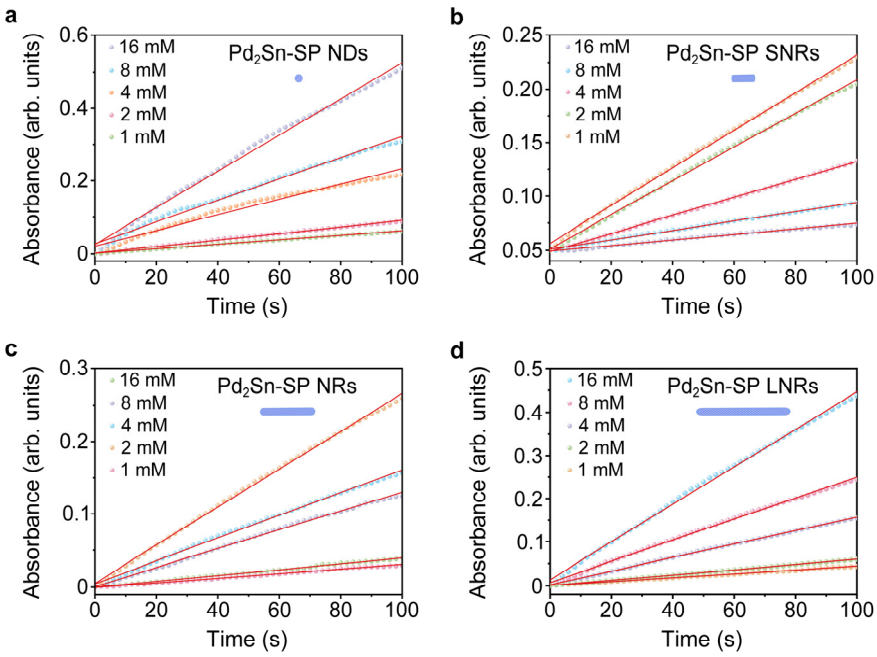

Supplementary Fig. 13. The initial linear portion *versus* the reaction-time curves. **a** Pd_2Sn-SP NDs, **b** Pd_2Sn-SP SNRs, **c** Pd_2Sn-SP NRs, and **d** Pd_2Sn-SP LNRs in the presence of H_2O_2 with various concentrations (n = 3 independent experiments). Source data are provided as a Source Data file (arb. units, arbitrary units).

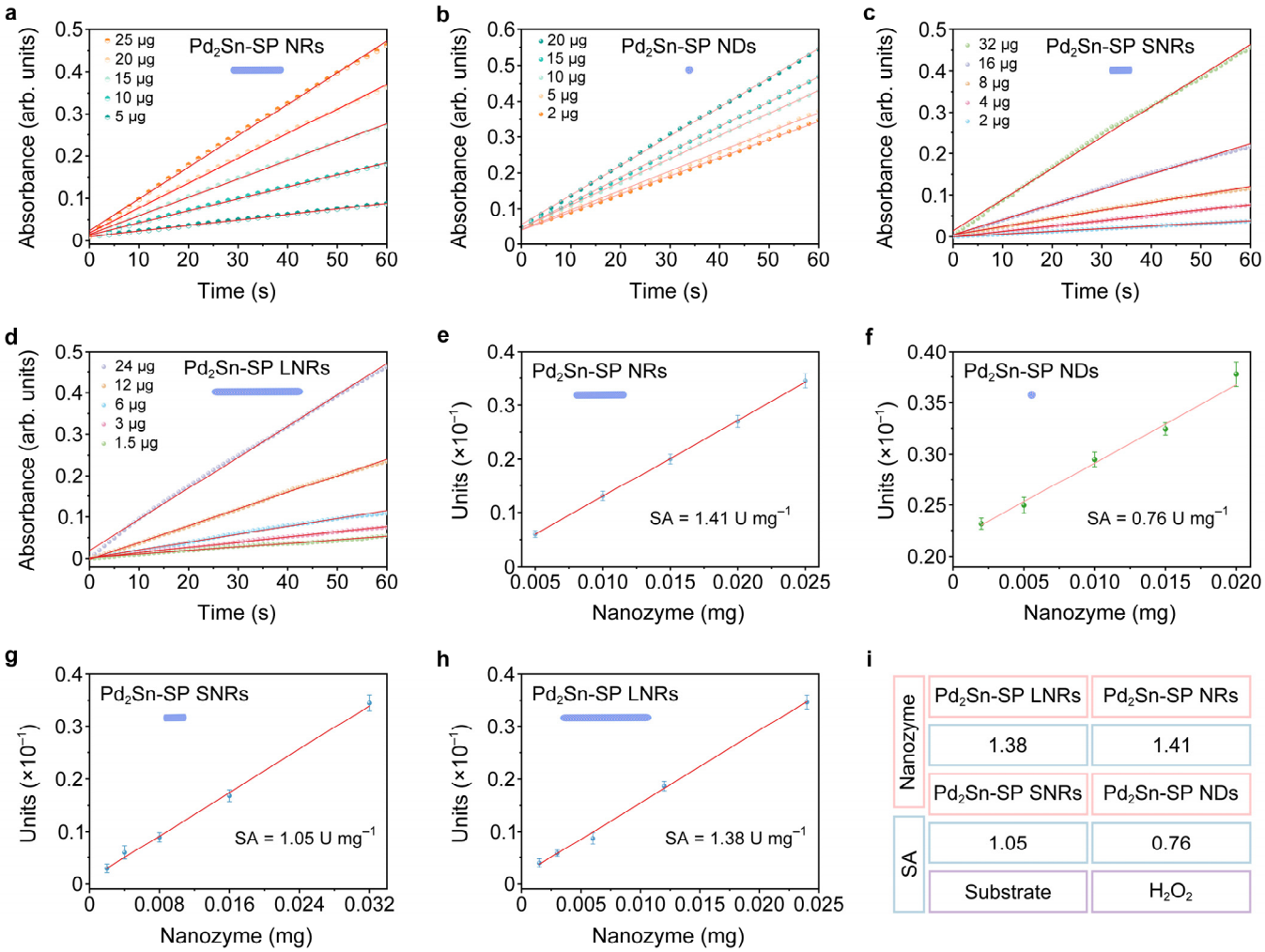

Supplementary Fig. 14. Specific activity analysis of Pd_2Sn-SP. The initial linear portion *versus* reaction–time curves of **a** Pd_2Sn-SP NRs, **b** Pd_2Sn-SP NDs, **c** Pd_2Sn-SP SNRs, and **d** Pd_2Sn-SP LNRs in the presence of H_2O_2 for various amounts. Specific activities of **e** Pd_2Sn-SP NRs, **f** Pd_2Sn-SP NDs, **g** Pd_2Sn-SP SNRs, and **h** Pd_2Sn-SP LNRs. **i** Comparison of the specific activity for Pd_2Sn-SP with different morphologies. Data are expressed as mean ± S.D. (n = 3 independent experiments). Source data are provided as a Source Data file (arb. units, arbitrary units).

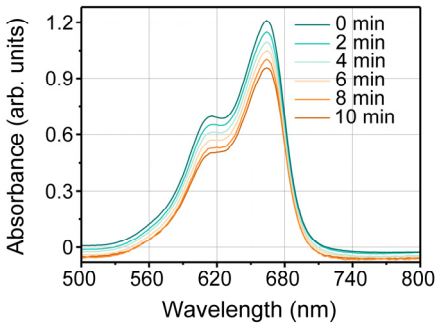

Supplementary Fig. 15. The degradation of MB catalyzed by Pd_2Sn-SP NRs at different time points (n = 3 independent experiments). Source data are provided as a Source Data file (arb. units, arbitrary units).

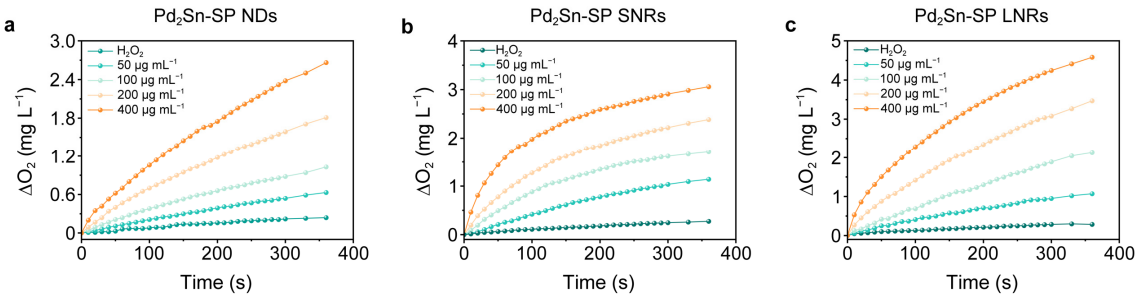

Supplementary Fig. 16. O_2 production performance of Pd_2Sn-SP. O_2 generation curves of **a** Pd_2Sn-SP NDs, **b** Pd_2Sn-SP SNRs, and **c** Pd_2Sn-SP LNRs with various concentrations (n = 3 independent experiments). Source data are provided as a Source Data file.

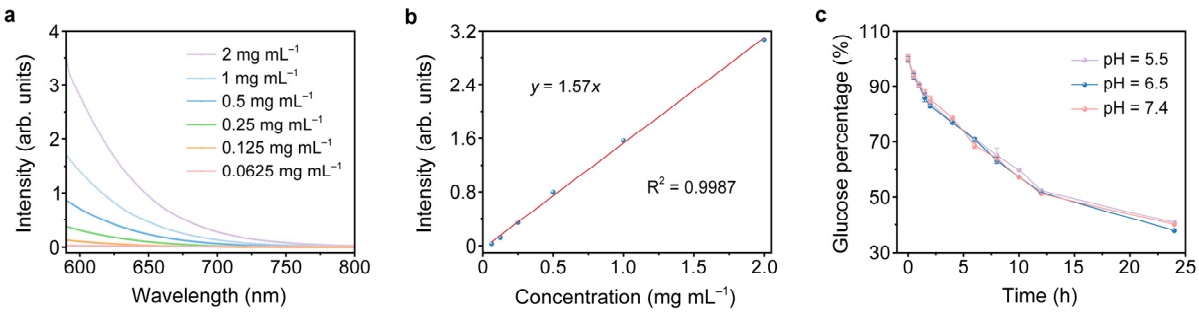

Supplementary Fig. 17. Glucose oxidase activity. a UV-vis-NIR absorption spectra of glucose at different concentrations after being reacted with dinitrosalicylic acid reagent. **b** The fitting curve of glucose concentration and absorbance at 595 nm. **c** Glucose consumption with the change of time at different pH values (n = 3 independent experiments). Source data are provided as a Source Data file (arb. units, arbitrary units).

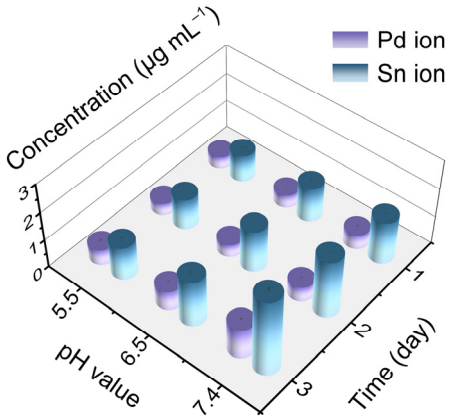

Supplementary Fig. 18. Evaluation of ions release performance. The release of Pd and Sn ions from Pd_2Sn@GOx-SP in PBS with various pH values during the incubation process. Data are expressed as mean ± S.D. (n = 3 independent experiments). Source data are provided as a Source Data file.

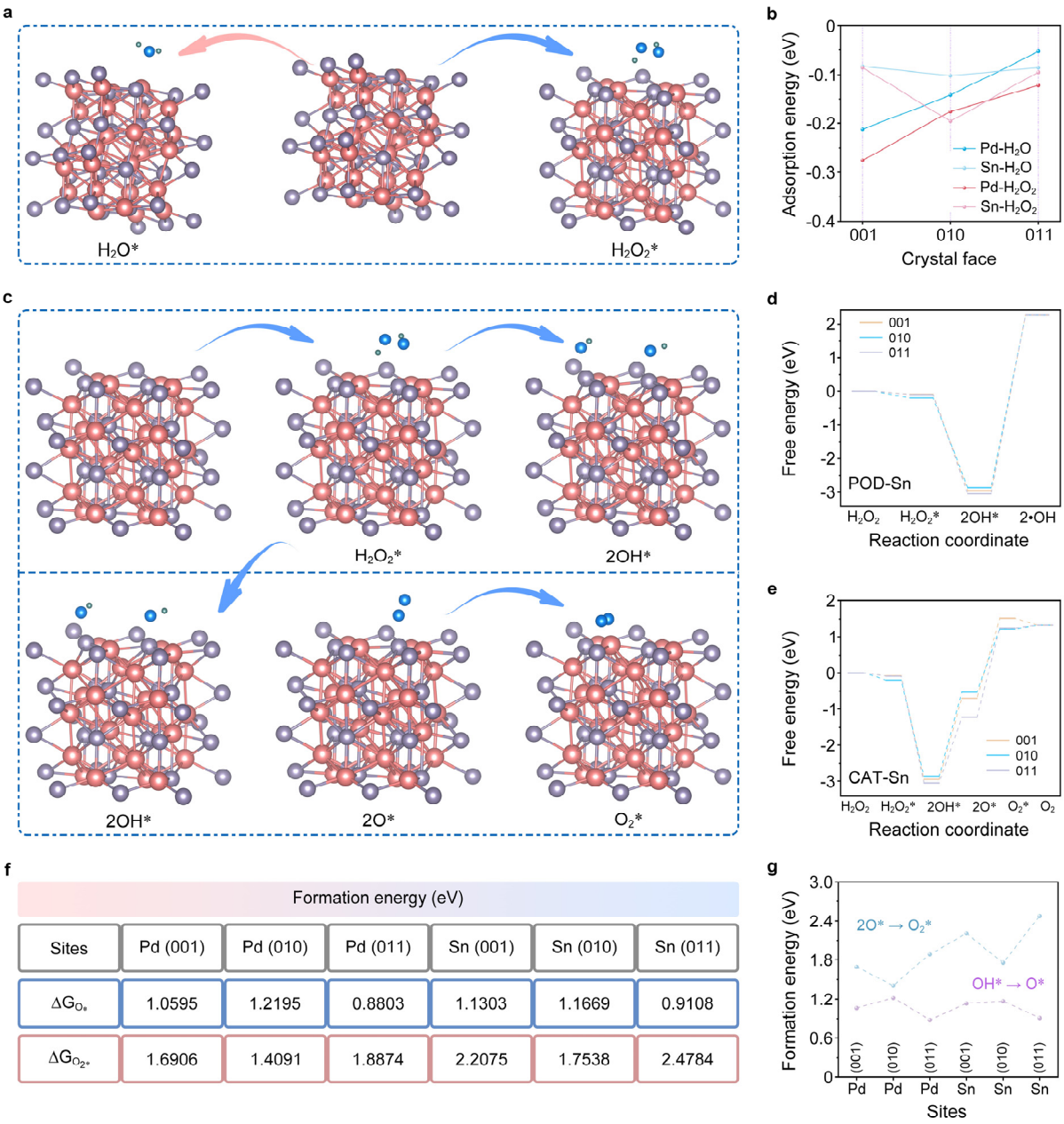

Formation energy (eV)						
Sites	Pd (001)	Pd (010)	Pd (011)	Sn (001)	Sn (010)	Sn (011)
ΔG_{O_*}	1.0595	1.2195	0.8803	1.1303	1.1669	0.9108
$\Delta G_{O_{2*}}$	1.6906	1.4091	1.8874	2.2075	1.7538	2.4784

Supplementary Fig. 19. DFT explorations on the POD- and CAT-mimic activities of Pd_2Sn. a The theoretical model and **b** adsorption energy of H_2O^* and $H_2O_2^*$ intermediates on the Pd and Sn sites of Pd_2Sn with different crystal facets. **c** The reaction pathways and **d, e** corresponding energy profiles for the POD- and CAT-mimic activities on Sn sites of Pd_2Sn with different crystal facets. **f, g** The formation energy of O* and O_2^* on the Pd and Sn sites of Pd_2Sn with different crystal facets. Source data are provided as a Source Data file.

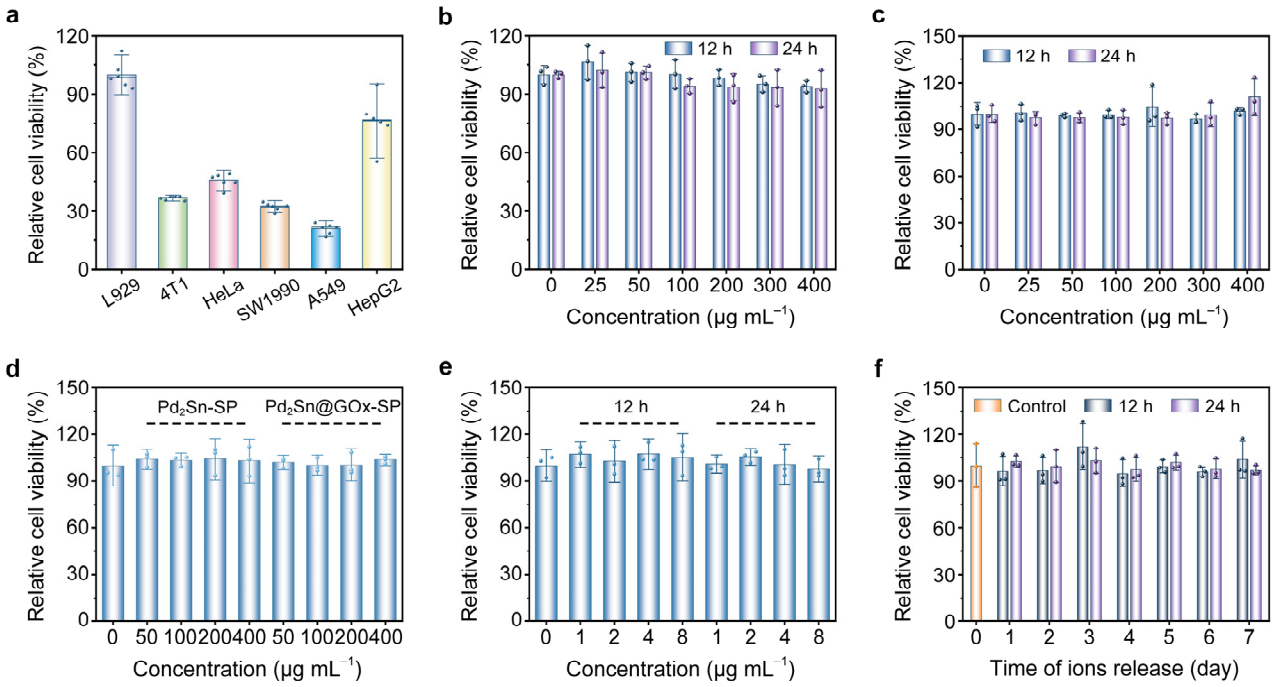

Supplementary Fig. 20. In vitro biosafety and toxicity analysis. a Relative cell viability of multiple cell lines after being treated with Pd_2Sn@GOx-SP plus laser. Data are expressed as mean ± S.D. (n = 6 independent samples). Relative cell viability of **b** L929 and **c** 3T3 cells after incubation with Pd_2Sn@GOx-SP for 12 and 24 h. Data are expressed as mean ± S.D. (n = 3 independent samples). **d** Relative cell viability of L929 cells incubated with Pd_2Sn-SP and Pd_2Sn@GOx-SP at various concentrations for 24 h. Data are expressed as mean ± S.D. (n = 3 independent samples). **e** Relative cell viability of L929 cells after incubation with TOP at different concentrations for 12 and 24 h. Data are expressed as mean ± S.D. (n = 3 independent samples). **f** Relative cell viability of L929 cells after incubation with Sn and Pd ions released from Pd_2Sn@GOx-SP. Data are expressed as mean ± S.D. (n = 3 independent samples). Source data are provided as a Source Data file.

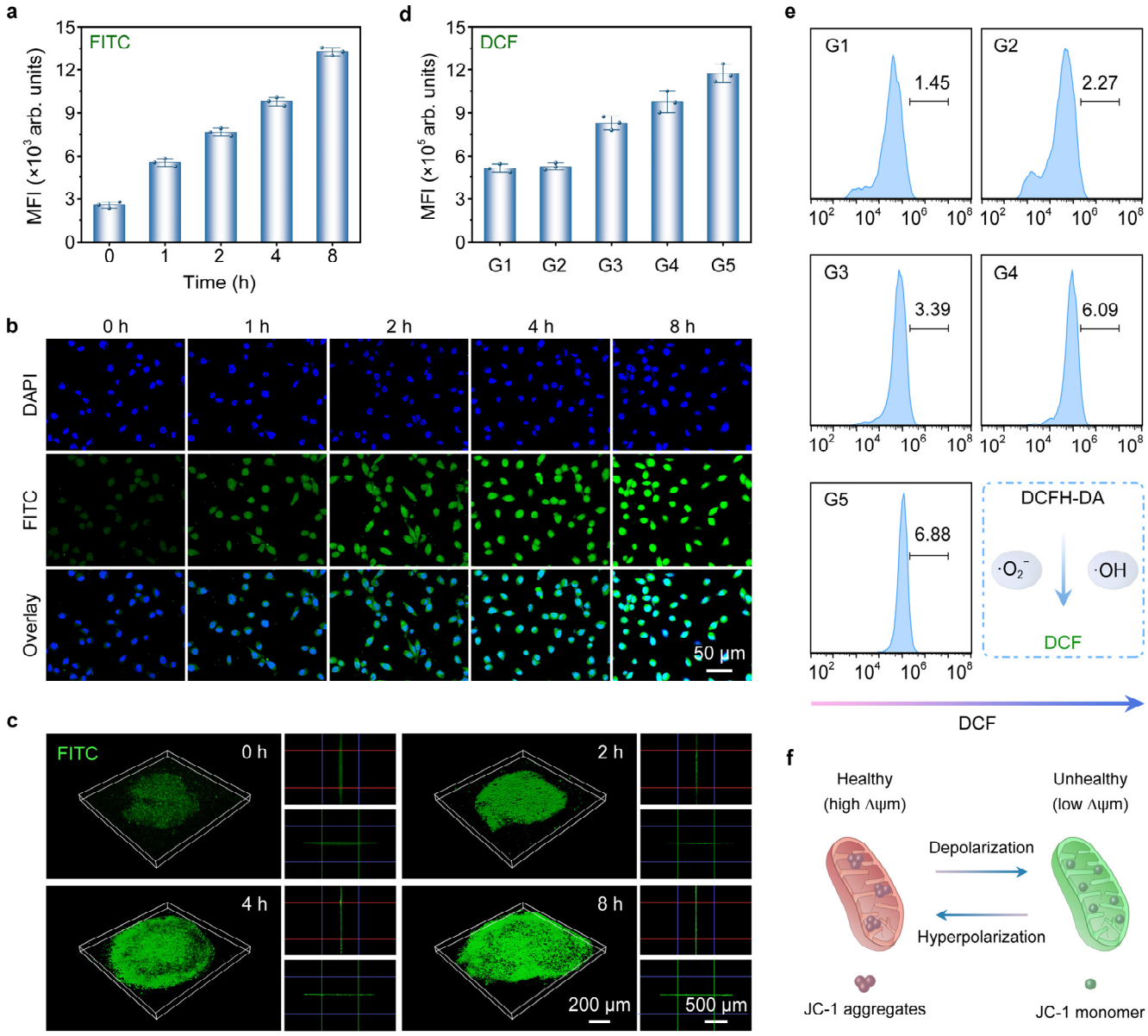

Supplementary Fig. 21. Uptake of Pd_2Sn@GOx-SP and intracellular ROS analysis. a The corresponding quantitative analysis of the mean fluorescence intensity in CT26 cells incubated with FITC-labeled Pd_2Sn@GOx-SP at different time points. CLSM fluorescence images of **b** CT26 cells and **c** CT26 multicellular spheroids incubated with FITC-labeled Pd_2Sn@GOx-SP at different time points. (one representative data was shown from three independently repeated experiments). **d,e** Flow cytometry profile and the corresponding mean fluorescence intensity of intracellular ROS level with different treatments (G1, control; G2, laser; G3, Pd_2Sn-SP; G4, Pd_2Sn@GOx-SP; G5, Pd_2Sn@GOx-SP + laser). **f** Schematic illustration of JC-1 staining for the change of mitochondrial membrane potential. Data are expressed as mean ± S.D. (n = 3 independent samples). Source data are provided as a Source Data file (arb. units, arbitrary units).

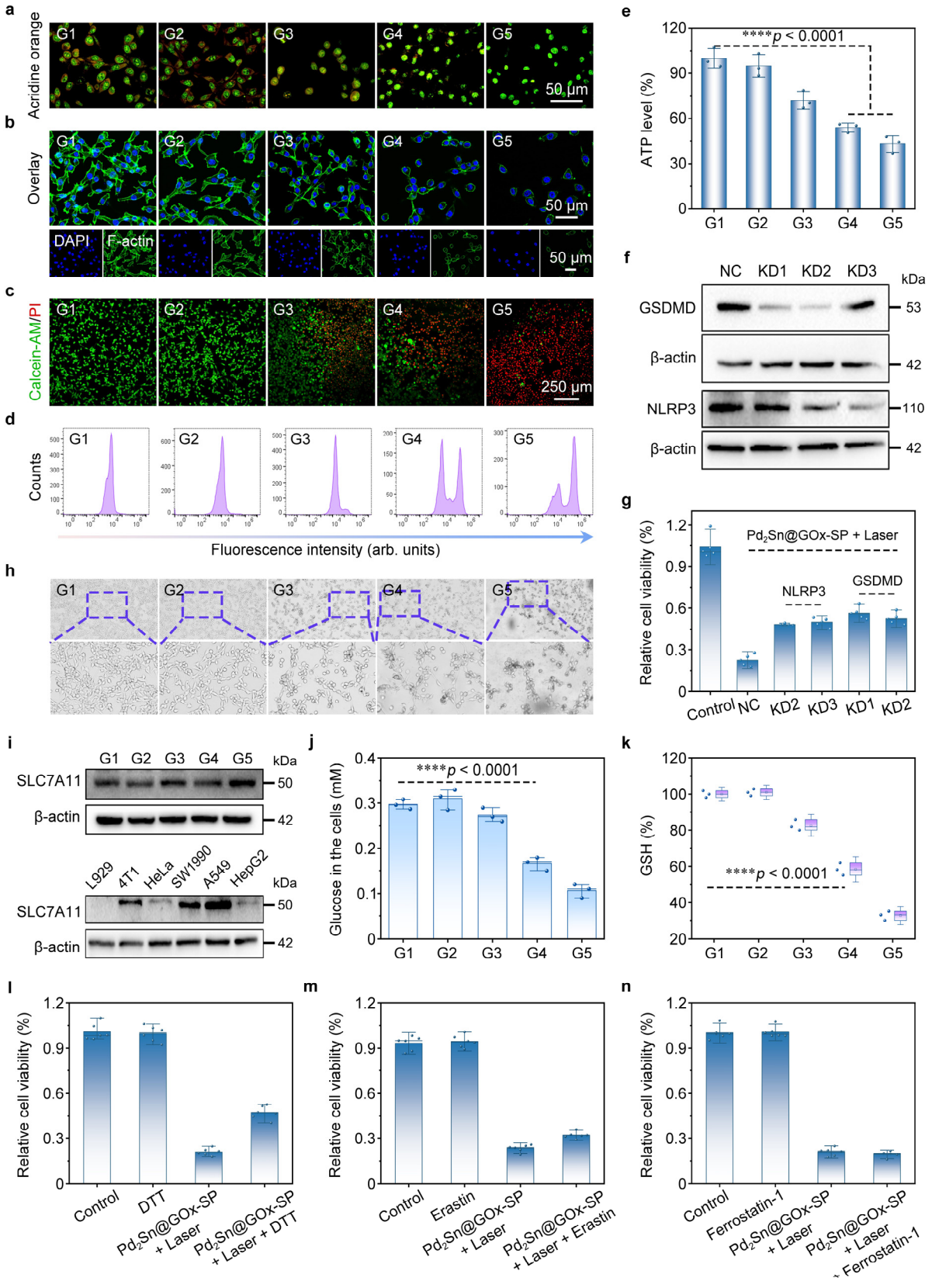

Supplementary Fig. 22. In vitro anticancer performance of Pd_2Sn@GOx-SP. a Acridine orange staining, **b** F-actin morphology, and **c** Calcein-AM/PI co-staining images of CT26 cells with various treatments (G1, control; G2, laser; G3, Pd_2Sn-SP; G4, Pd_2Sn@GOx-SP; G5, Pd_2Sn@GOx-SP + laser). **d** Flow cytometry analysis of the living and dead cells proportion after various treatments. **e** Intracellular ATP levels after diverse

treatments. Data are expressed as mean ± S.D. (n = 3 independent samples). **f** Protein levels of NLRP3 and GSDMD in NLRP3- or GSDMD-knockdown CT26 cells by using western bolt analysis. **g** Relative cell viability of NLRP3-knockdown or GSDMD-knockdown CT26 cells treated with Pd_2Sn@GOx-SP + laser. Data are expressed as mean ± S.D. (n = 5 independent samples). **h** Bright-field cell morphology after diverse treatments. **i** Protein levels of SLC7A11 in CT26 cells (upper panel) and multiple cell lines (bottom panel). (one representative data was shown from three independently repeated experiments). **j** Glucose content and **k** GSH depletion in different treatment groups. Data are expressed as mean ± S.D. (n = 3 independent samples). Relative cell viability of CT26 cells upon Pd_2Sn@GOx-SP + laser treatment with the addition of **l** DTT, **m** Erastin, and **n** Ferrostatin-1. Data are expressed as mean ± S.D. (n = 6 independent samples). Statistical significance is assessed by a two-way ANOVA with Tukey's multiple comparisons test. Source data are provided as a Source Data file (arb. units, arbitrary units).

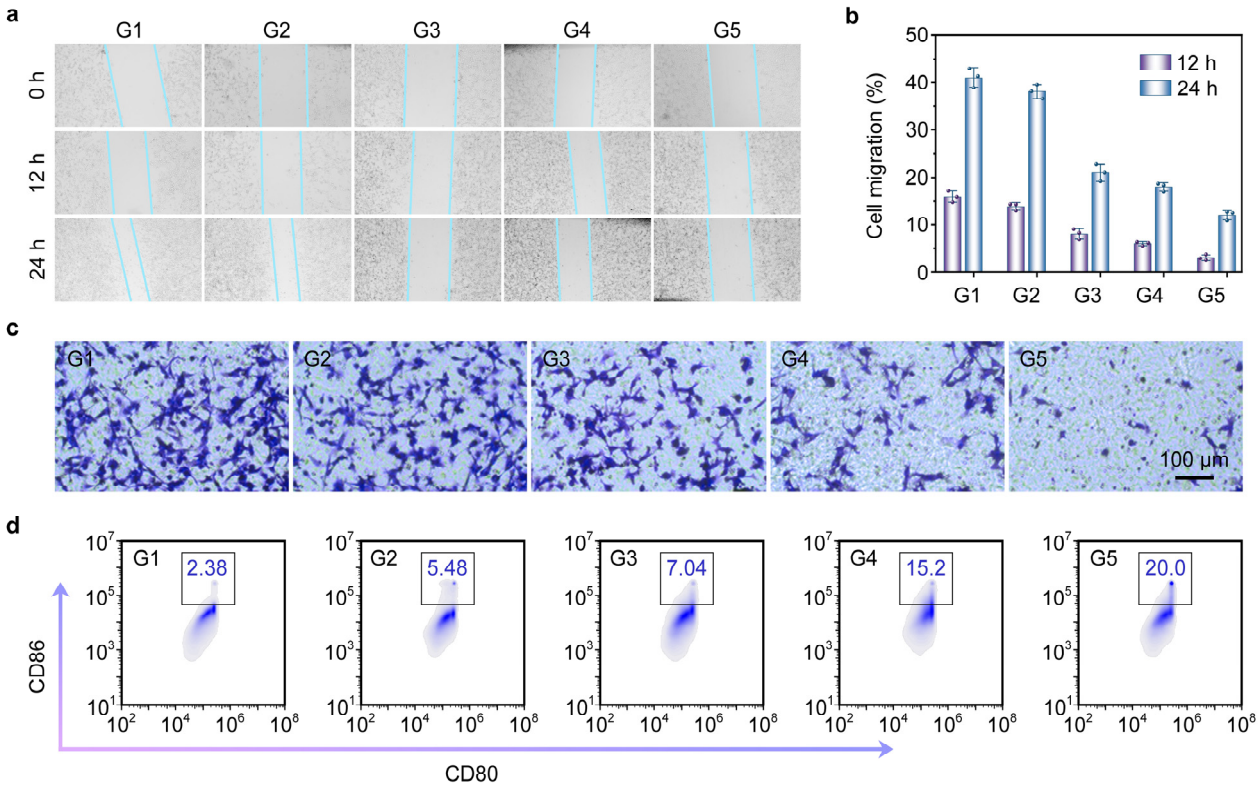

Supplementary Fig. 23. Cell migration and immune stimulation analysis. a Wound-healing assays and **b** the corresponding quantitative analysis of CT26 cells treated with various formulations (G1, control; G2, laser; G3, Pd_2Sn-SP; G4, Pd_2Sn@GOx-SP; G5, Pd_2Sn@GOx-SP + laser) at different times. **c** The transwell migration assay of CT26 cells after diverse treatments. **d** Flow cytometry profiles of DCs maturation ($CD80^+$ and $CD86^+$ cells) after different treatments by in vitro stimulation maturation experiment. Data are expressed as mean ± S.D. (n = 3 independent experiments). Source data are provided as a Source Data file (one representative data was shown from three independently repeated experiments).

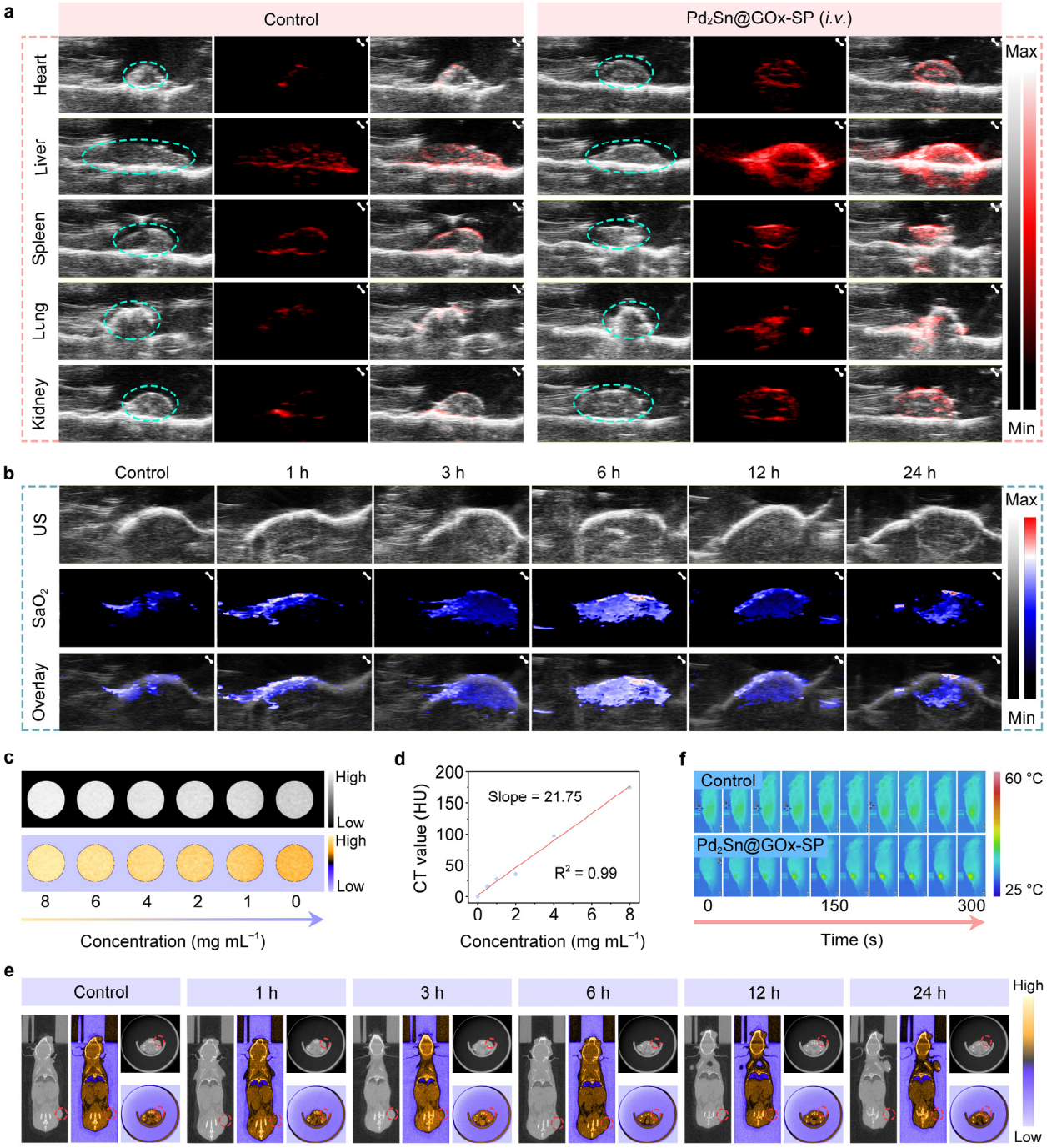

Supplementary Fig. 24. Imaging performance evaluation of Pd_2Sn@GOx-SP. a PA images of various organs collected from the representative mice before and after 6 h of injection. **b** In vivo PA images of SaO_2 in the tumor region after *i.v.* injected with Pd_2Sn@GOx-SP at different time intervals. **c** In vitro CT pseudocolor images of Pd_2Sn@GOx-SP at different concentrations. **d** CT values of Pd_2Sn@GOx-SP at different concentrations. **e** In vivo coronal and transverse sections of tumor area after *i.v.* injected with Pd_2Sn@GOx-SP at different time intervals. The left and right columns show pseudo-color images and grayscale images, respectively. **f** Time-dependent in vivo thermal imaging of mice at the tumor region after

i.v. injected with PBS or Pd_2Sn@GOx-SP. Source data are provided as a Source Data file (one representative data was shown from three independently repeated experiments).

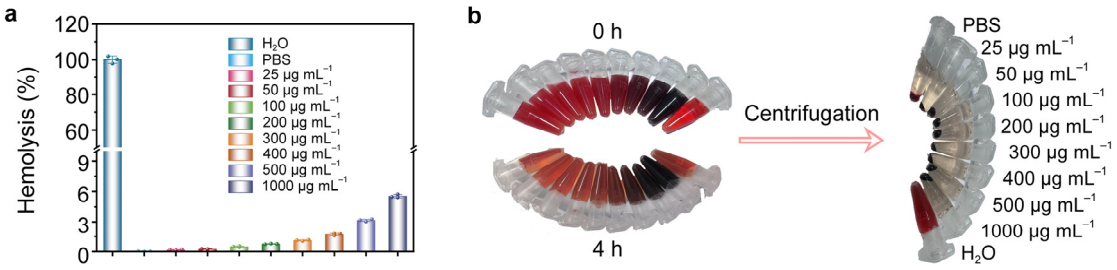

Supplementary Fig. 25. Hemolysis of red blood cells after incubating with Pd_2Sn@GOx-SP. a Hemolysis rate after incubation with different concentrations of Pd_2Sn@GOx-SP and **b** the corresponding digital photograph incubated with various concentrations of Pd_2Sn@GOx-SP, PBS (negative control), and water (positive control). Data are expressed as mean ± S.D. (n = 3 independent experiments). Source data are provided as a Source Data file.

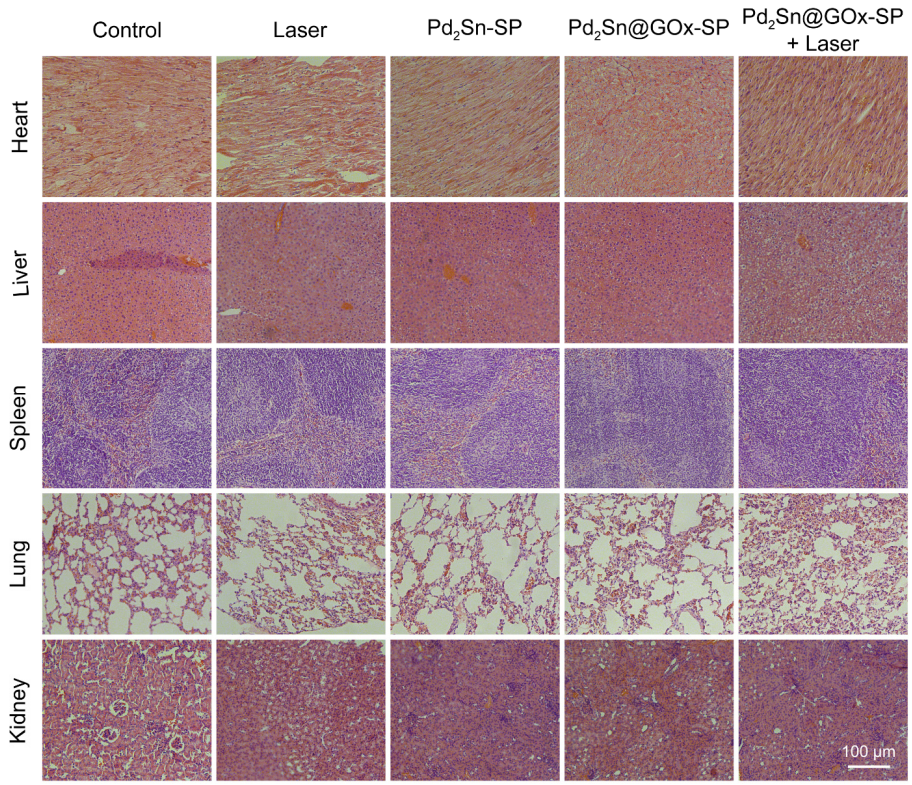

Supplementary Fig. 26. H&E staining images for heart, liver, spleen, lung, and kidney of mice in different groups. (one representative data was shown from three independently repeated experiments).

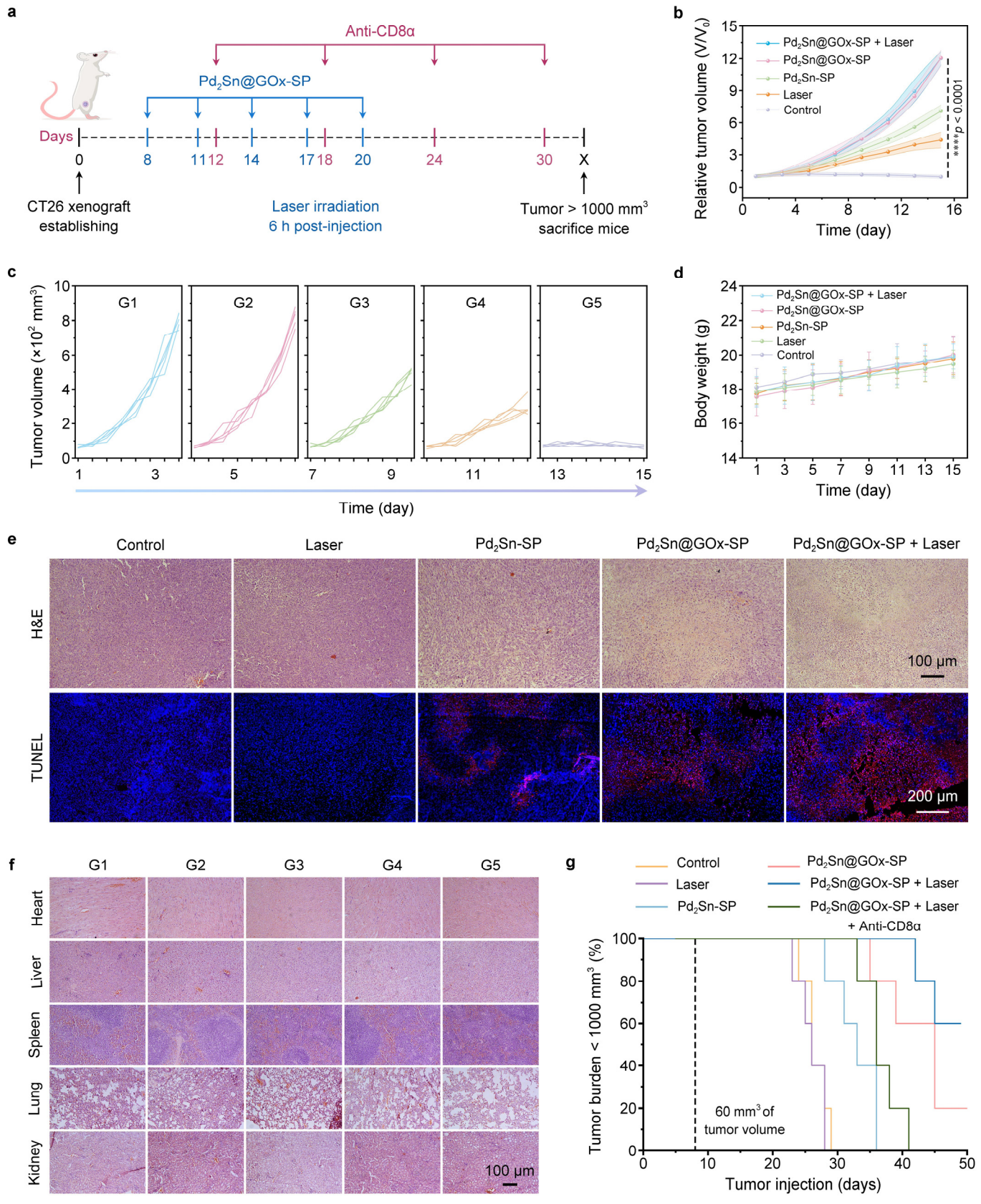

Supplementary Fig. 27. In vivo synergistic antitumor therapy on 4T1 tumor-bearing mice. a Treatment schedule for mice receiving nanocomposites or CD8-depleting antibodies (Anti-CD8α). **b** Relative tumor volume, **c** tumor volume, and **d** body weight of the mice in different treatment groups (G1, control; G2, laser; G3, Pd_2Sn-SP; G4, Pd_2Sn@GOx-SP; G5, Pd_2Sn@GOx-SP + laser). Data are expressed as mean ± S.D. (n =

5 mice for each group). **e** H&E and TUNEL staining images of tumor tissue slices from the representative mice in different treatment groups. **f** H&E staining images of heart, liver, spleen, lung, and kidney collected from the representative mice in different treatment groups. 5 times each experiment was repeated independently with similar staining images. **g** Kaplan-Meier survival graph of mice receiving various formulations. Statistical significance is assessed by a two-way ANOVA with Tukey's multiple comparisons test. Source data are provided as a Source Data file (one representative data was shown from three independently repeated experiments).

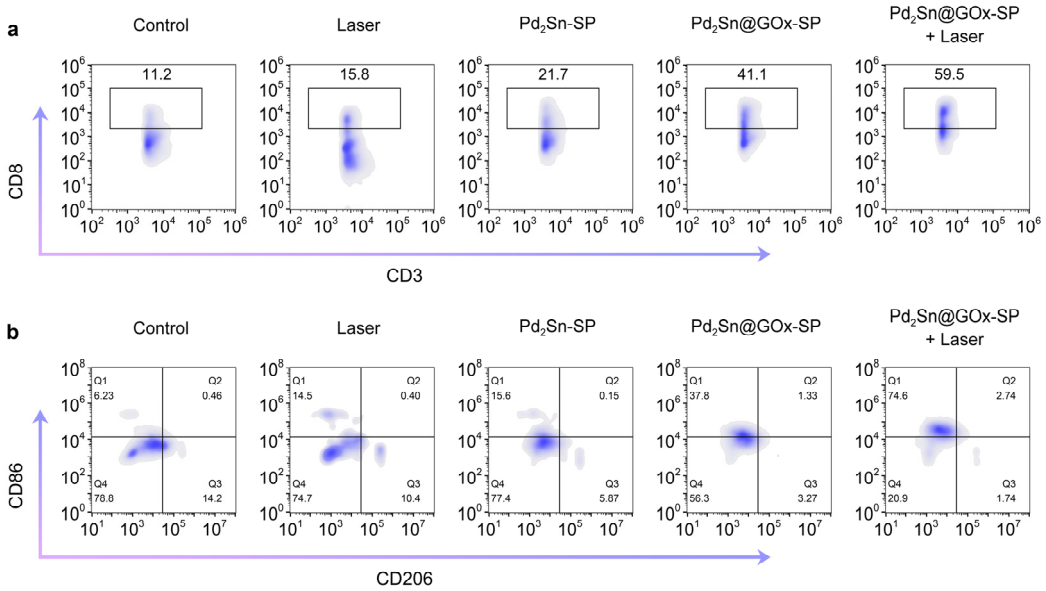

Supplementary Fig. 28. Flow cytometry analysis of immune cells in vivo. Representative flow cytometric images of **a** $CD8^+$ T cells and **b** M2-type macrophages ($CD86^-$ and $CD206^+$) and M1-type macrophages ($CD86^+$ and $CD206^-$) in tumor tissues after receiving different treatments (n = 3 independent samples).

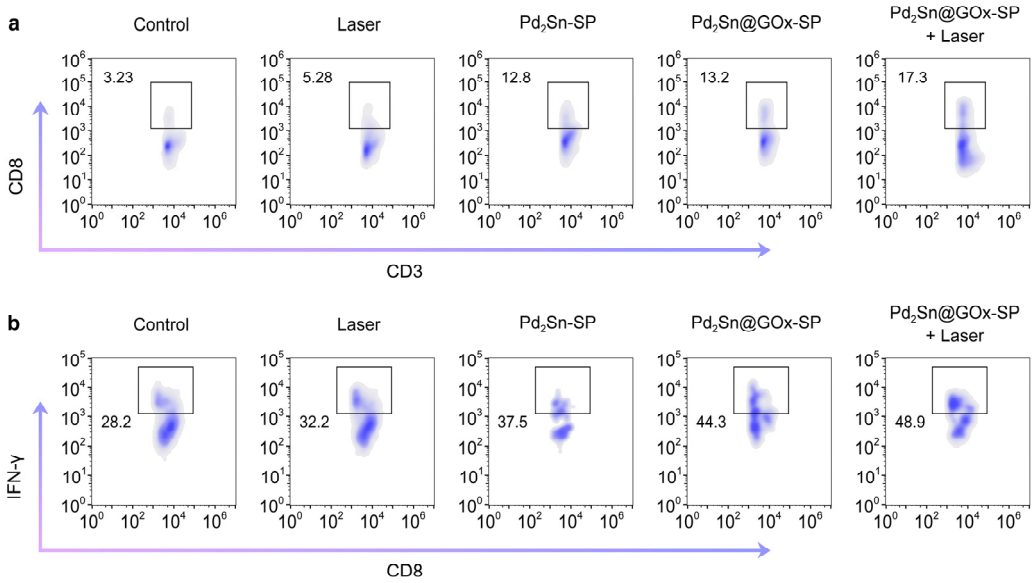

Supplementary Fig. 29. Flow cytometry analysis of immune cells after various treatments. Representative flow cytometric images of **a** $CD8^+$ T cells and **b** IFN-γ in distal tumor tissues after receiving different treatments(n = 3 independent samples).

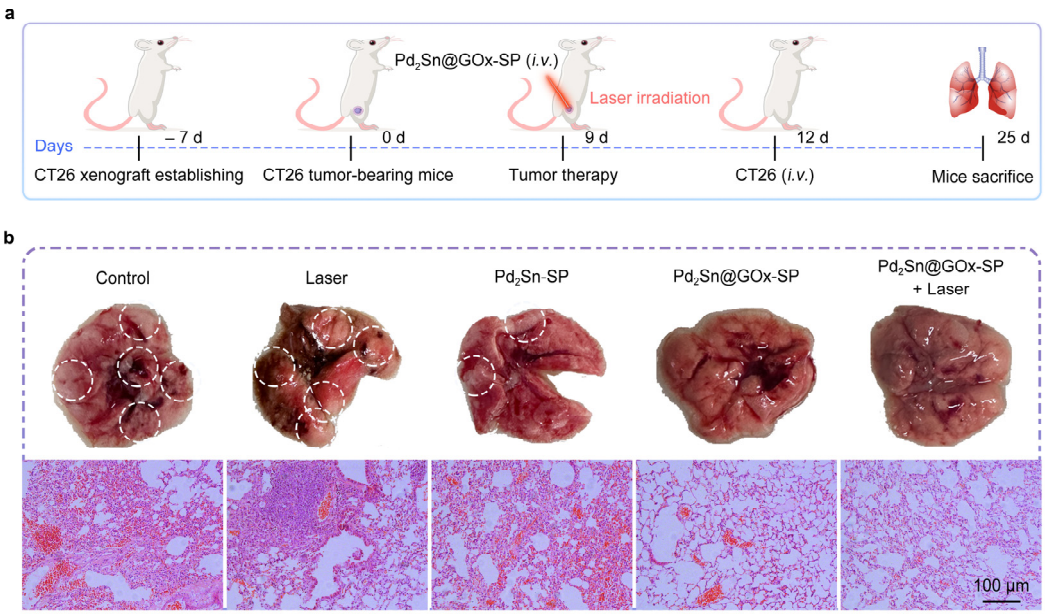

Supplementary Fig. 30. Synergistic therapy inhibited tumor metastasis. a Schematic illustrations of tumor lung metastasis experiment. **b** Representative images of the whole lungs and H&E staining images of lung tissues treated with different formulations. (one representative data was shown from three independently repeated experiments).

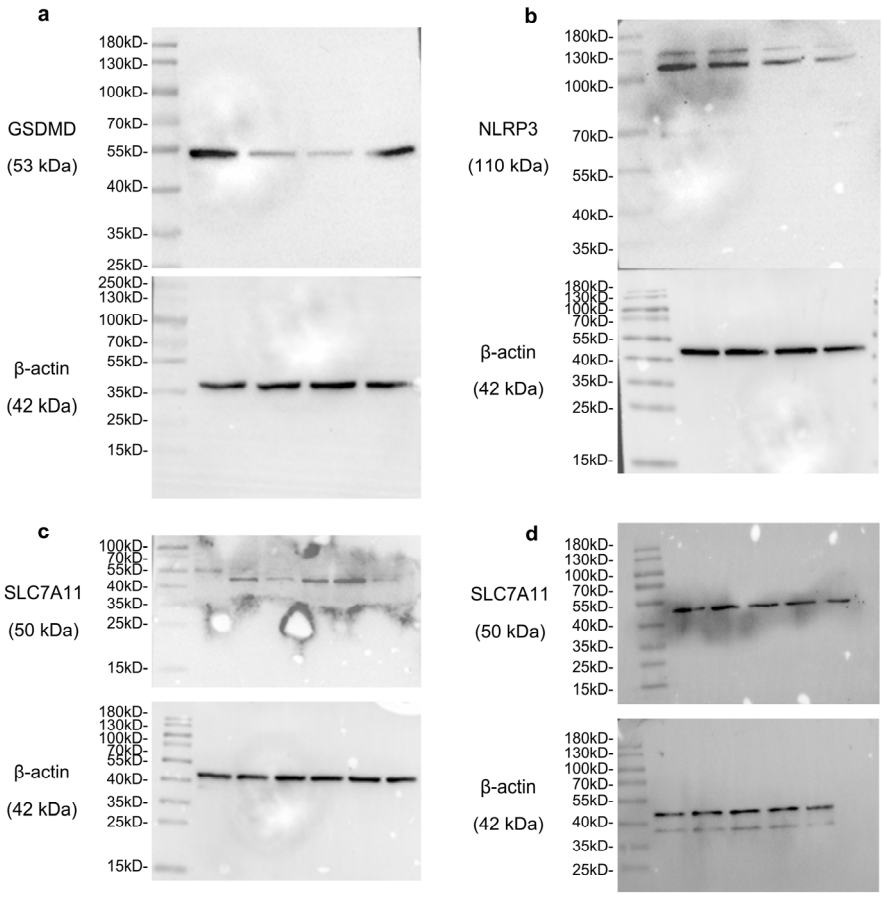

Supplementary Fig. 31. The uncropped scans of all blots and gels for GSDMD, NLRP3, and SLC7A11.

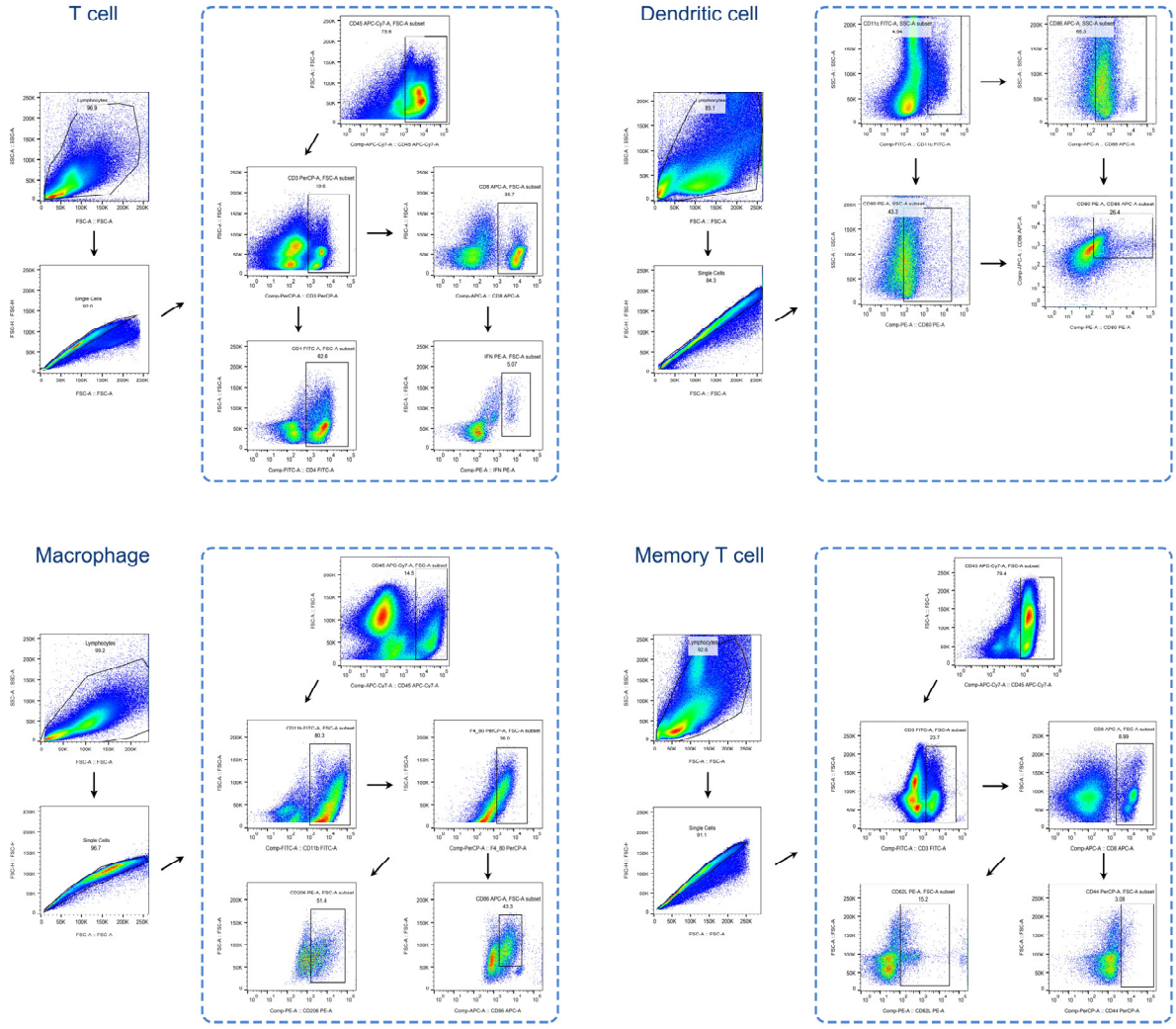

Supplementary Fig. 32. Representative gating strategies for analyzing T cell, dendritic cell, macrophage, and memory T cell.